Generation of High-Order Waveguide Modes with Reduced Symmetric Protection

Jianfeng Chen,[1,*] Qiang Cheng,[1,*,†] Wei Yuan,[1] Li Wang,[1] Wen Xuan Tang,[1] Lei Wang,[2] and Tie Jun Cui[1,‡]

[1] *State Key Laboratory of Millimeter Waves, Department of Radio Engineering, Southeast University, Nanjing 210096, People's Republic of China*

[2] *School of Engineering and Physical Sciences, Heriot-Watt University, Edinburgh EH14 4AS, United Kingdom*

(Received 23 January 2020; revised 8 April 2020; accepted 22 July 2020; published 14 August 2020; corrected 4 November 2020)

Single-mode operation in a rectangular waveguide is very important, since the existence of multimodes may arouse distortions of carried signals due to the modal dispersion. High-order mode means multiple periods of field in the transverse cross section, with distinct electromagnetic properties from the dominant mode. Although numerous methods are proposed to achieve mode selection within the waveguide, they only permit specific high-order modes to survive in a frequency range. However, it still remains a great challenge to control the bandwidth freely for single-mode operation. Here, we propose an approach for high-order mode generation, in which the desired mode operates in the band gap of other modes, and the working bandwidth can be engineered independently by reducing the symmetry of the loaded periodic metallic ridges in the waveguide. Two examples are demonstrated, where only TE_{20} and TE_{30} modes are supported. The proposed method can also be applied to generate other high-order TE modes in the future.

DOI: 10.1103/PhysRevApplied.14.024040

I. INTRODUCTION

Waveguides, as an important family of transmission lines to route electromagnetic waves and convey energy between two endpoints, are widely employed to realize many microwave or optical components, including filters, couplers, isolators, resonators, antennas, and power dividers, showing the advantages of low transmission loss, broad bandwidth, and high power-handling capability. Initially, single-mode operation is essential to achieve a high transmission efficiency and stable system performance, where tremendous efforts are made to suppress high-order modes and improve the single-mode bandwidth [1–6]. However, with the rapid advance of waveguide technology, the high-order modes have gained increasing interest and witnessed successful applications, such as power combining, high-power electron devices, microwave heating, and millimeter wave antennas [7–19].

In general, when we deal with high-order modes in traditional waveguides, the fundamental mode usually also exists, making it hard to extract the desired order mode for device and antenna design. To overcome this limitation, several approaches are proposed to realize high-order mode generation. One way is to introduce discontinuities inside the waveguide. For instance, a right-angled corner is used to connect two differently sized waveguides, so as to realize the conversion from TE_{10} to TE_{20} mode. Several metallic posts are placed in this corner to suppress the dominant TE_{10} mode [20–23]. Another option to reach that goal is to shift the feeding point some distance from the center, which can enhance the intensity of the TE_{20} mode and suppress the generation of the TE_{10} mode [24].

Here, we report on an alternative method to generate a single high-order mode in a rectangular metallic waveguide with symmetric protection technology. To eliminate the fundamental TE_{10} of the rectangular waveguide, periodic metallic ridges are loaded at the top and bottom waveguide surfaces to form a band gap for the TE_{10} mode within the spectrum of interest, where only the desired TE_{20} mode can survive. The reduced glide symmetry of the ridges is introduced to adjust symmetric protection in the proposed waveguide, since the degree of glide symmetry breaking determines the range of the band gap for the fundamental mode, with the band-gap center unchanged. Thereby, it allows us unprecedented control over the propagation characteristics of the single high-order mode, such as the working bandwidth and central operation frequency. Similarly, the generation of a single TE_{30} mode is also implemented in theory and experiments, by controlling the dimensions of the periodically loaded ridges. In contrast to the reported high-order-mode-converting strategies of recent decades [22–24], our scheme stands out as for its simple structure, easy implementation, customized bandwidth, and high mode purity, which provide exceptional flexibility for mode manipulation in engineering. To confirm the validity of our findings, both numerical and

*These authors contributed equally to this work.
†qiangcheng@seu.edu.cn
‡tjcui@seu.edu.cn

experimental studies are carried out to investigate the mode properties of a ridge-loaded rectangular waveguide. By engineering reduced glide symmetry of the ridges, we verify the feasibility of single high-order mode generation in the microwave region. Due to the advantages of high-order TE_{n0} mode purity and easy design of the proposed structure, we believe that this investigation provides inspiration for the application of one-to-n power dividers and phase shifters, especially in the millimeter wave band, since electric separations between adjacent channels can be removed, which is helpful for simplifying the geometry.

II. THEORY AND DESIGN

The electromagnetic (EM) field distributions within a waveguide can be obtained by solving wave equations with the corresponding boundary conditions. In general, knowledge of the longitudinal components for both electric and magnetic fields is sufficient to determine the total fields inside the waveguide [25]. For a guided wave structure with a regular cross section, there exist a number of discrete solutions with regard to the wave equations, corresponding to various waveguide modes in reality. Each mode is associated with a cutoff frequency, beyond which the mode can propagate with little attenuation within the waveguide. Take the rectangular waveguide in Fig. 1(a), for example, the coexistence of the first- and second-order modes can be clearly observed at high frequencies from the gray region of the modal dispersion diagram in Fig. 1(b). In fact, the first-order mode can never be efficiently removed due to the lowest cutoff frequency, implying that it is hard for the high-order mode to exist inside the waveguide on its own.

To circumvent this problem and change the mode dispersions, we need to modify the boundary conditions of the waveguide, giving rise to the desired mathematical representations of solutions to the wave equations. Here, we consider the rectangular waveguide loaded by periodic structures, which is widely applied in microwave engineering to realize functionalities such as microwave filters, traveling-wave antennas, and microwave tubes. For the periodic structure in Fig. 1(c), it supports a set of Bloch modes that are closely related to structural symmetry, according to the Floquet theorem [26–28]. Under this circumstance, the waveguide loaded with periodic structures behaves as a one-dimensional (1D) photonic crystal, which is featured by the emergence of the band gap in which the original waveguide mode is no longer supported due to multiple scattering between the unit cells. As illustrated in Fig. 1(d), the dispersion curve of the original fundamental mode (TE_{10} mode) is split into a set of spatial harmonics [29], with the formation of band gaps at the split point, where $\beta L = n\pi$ (L is the loading period, n is an integer) [29]. Additionally, the high-order modes are often found to exist out of the band gap. As a result, it makes the periodically loaded waveguide a good candidate for the band-rejection filter in engineering, which has been extensively investigated in the literature in the past two decades [30,31].

However, a question then naturally arises whether the specific high-order waveguide mode can fall into the band gap of the fundamental mode, as shown in Fig. 1(e), since it would offer an efficient avenue to realize a single high-order mode operation that is extremely desired in many situations. Actually, as revealed by numerical simulations, this goal can be achieved by carefully optimizing the element shapes and dimensions, and we successfully

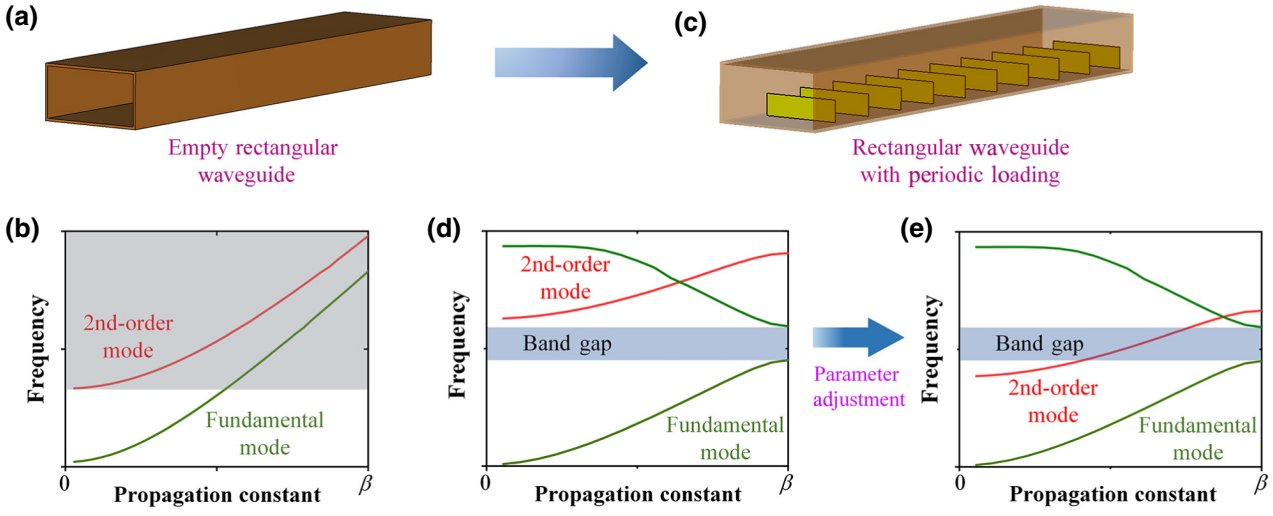

FIG. 1. (a),(b) Schematic of an empty rectangular waveguide and corresponding dispersion diagram. (c)–(e) Schematic of a rectangular waveguide with periodic loading, and corresponding dispersion diagrams before and after parameter adjustment.

demonstrate the feasibility of allocating the desired high-order mode into the apparently forbidden region. This makes sense because, for an infinitely periodic structure, the upper and lower edge frequencies of the band gap can be calculated by using the Bragg diffraction condition, as

$$2\mathbf{k}\cdot\mathbf{G} = G^2, \tag{1}$$

where $\mathbf{k}$ is the wave vector (corresponding to β in the 1D period system) and $\mathbf{G}$ is the reciprocal vector of the period lattice. Notably, the wave vector for each mode is distinct, showing the diversity of Bragg diffraction conditions for different modes. Therefore, each stop band works only for its corresponding mode.

Next, we proceed to investigate the feasibility of bandwidth control for single high-order mode operation. It is well known that the band gap of the fundamental mode can be adjusted by altering the geometry of the unit cell and the periodicity. However, a change to the structural dimensions usually leads to the offset of the band-gap center [20–24], despite the possibility of the band-gap width being effectively modified, and therefore, greatly limits its applicability to reconfigurable devices.

Indeed, an additional degree of freedom can be introduced to customize the band-gap bandwidth, while retaining a stable central frequency, which explores the variation of element symmetry along the propagation direction of the guided waves. Specifically, a periodically loaded structure is said to possess glide symmetry if it is coincident with itself under the glide operation, G, as follows [29,32]:

$$G = \begin{cases} x \to -x \\ y \to y \\ z \to z + L/2 \end{cases}, \tag{2}$$

and the wave numbers of the periodic structure with normal and glide symmetry (β_T and β_G, respectively) are connected by

$$\beta_T L = \beta_G L + 2\pi\nu, \quad \nu = 0,\ 1, \tag{3}$$

where L is the periodicity and ν is a natural number [29]. When the glide symmetry is applied for the periodic structures, the band gap between the two branches of the dispersion curves can be eliminated from coupled-mode theory [29,33]. For a periodic structure with normal symmetry, the coupling between two harmonic modes can happen at points $\beta L = n\pi$. The power flow of one harmonic mode will be completely offset by the other. As a result, the net power flow equals zero based on the conservation of energy. The degeneracy point will split, assuming that there is no source of energy in the guiding structure. However, the harmonic branches are uncoupled at $\beta L = \pi$ for the case of glide symmetry. So, these uncoupled modes, corresponding to different branches of the dispersion curves, are able to cross (degeneracy) when ν is odd [33]. According to the difference of the dispersion characteristics for a periodic structure with normal and glide symmetry, it is rational to adjust the bandwidth by breaking glide symmetry of the elements, resulting in the disappearance of the degeneracy point and the formation of the expected stop bands. During the transition from glide symmetry to normal symmetry, the band-gap width is gradually increased with a fixed central frequency, which suggests that symmetry control offers an important tool to manipulate the band gap of the fundamental mode for high-order mode operation.

To validate the proposed theory, a periodically ridge-loaded rectangular waveguide is designed to realize high-order mode operation. In microwave engineering, the metallic ridge is widely employed to reduce the cutoff frequency of the fundamental mode and, thereby, minimize the dimensions of the cross section and achieve good impedance matching. However, here, we try to adjust the symmetry of the loaded metallic ridges to change the band-gap behavior, as depicted in Fig. 2(a). We consider the waveguide with lateral dimensions of 16 and 10 mm. The ridge length, width, and period are a, b, and L, respectively. The ridges are arranged alternatively on the top and bottom plates, as marked by red and green, respectively, in Fig. 2(a), with a separation distance of L_1. The full wave simulation package CST 2018 is used to observe the modal distributions inside the waveguide. Initially, when the glide symmetry of the loaded ridges is assumed to be $L_1 = L/2$, and only one ridge is placed in the lateral direction, the TE_{10} mode is generated as predicted by classical electromagnetic theory, as shown in Fig. 2(a). Interestingly, if the width of the waveguide is doubled transversely, with two ridges aligned side by side [see the bottom-right panel of Fig. 2(a)], the dominant mode changes into the TE_{20} mode, as depicted by the field distributions in the waveguide cross section in Fig. 2(b). By further increasing the waveguide width, to allow more ridges in the transverse direction, we clearly see excitation of the high-order TE_{30} and TE_{40} modes, revealing that the waveguide width is a critical issue to be considered for high-order mode generation.

In addition, the dispersion properties of the TE_{10} and TE_{20} modes are also studied with the dependence of the structural symmetry, as displayed in Fig. 2(d). With a decrease of the spatial shift L_1 from $L/2$ to zero, the glide symmetry is broken and normal symmetry is finally achieved when L_1 reaches zero. The electromagnetic band gap starts to arise for the TE_{10} mode and then becomes larger and larger as shift L_1 shrinks. On the contrary, only the TE_{20} mode can be supported within the gap, which offers the possibility of single-mode operation, as desired. It is worth noting that the central frequency is hardly affected by the change of the band gap, which provides great convenience for adjusting the bandwidth of the single high-order mode operation.

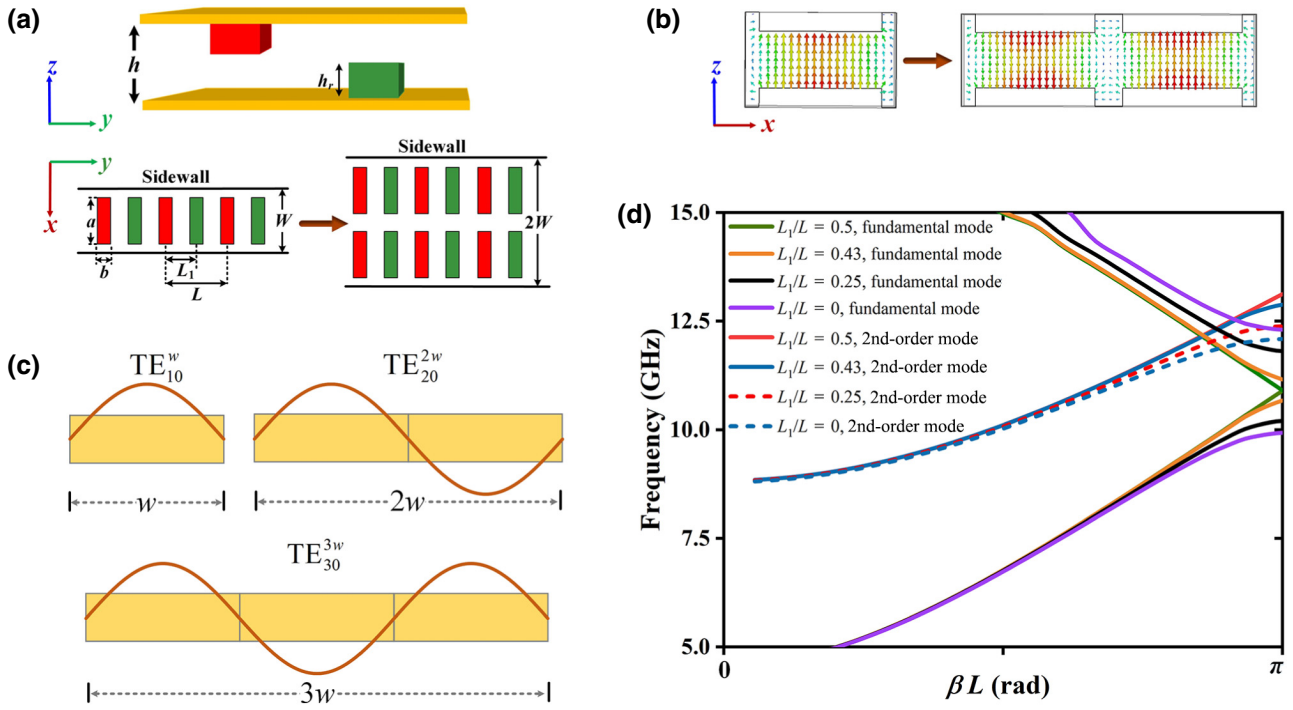

FIG. 2. (a),(b) Structural views of periodically loaded waveguides with one and two metallic ridges in the lateral direction ($h = 10$ mm, $h_r = 2$ mm, $L = 14$ mm, $W = 18$ mm, $a = 13$ mm, $b = 3$ mm, and $L_1 = 0$–7 mm) and the electric field distributions in the x-o-z cross section. (c) Electric field distributions of TE_{10}, TE_{20}, and TE_{30} modes with waveguide widths of w, $2w$, and $3w$, respectively. (d) Dispersion curves of the periodically loaded waveguide with two metallic ridges in the transverse direction.

One important aspect that needs to be further explored is excitation of the single high-order mode within the waveguide. Although the high-order mode can be produced by increasing the waveguide width, we observe that TE_{n0}^{nw} and TE_{10}^{w} have identical dispersion features in the Brillouin zones, where n is the mode index, and the superscript represents the corresponding waveguide width for better understanding. It is well known that the propagation

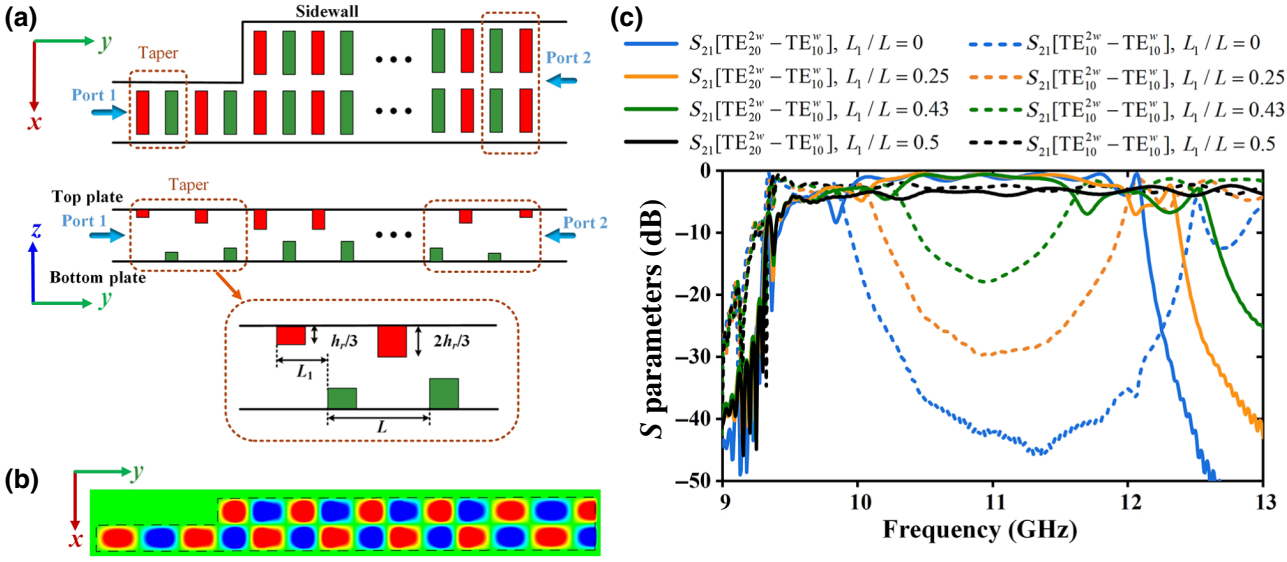

FIG. 3. (a) Top and side views of the TE_{20} mode generator, where dotted rectangles indicate taper regions with gradually changed ridges to improve impedance matching. (b) Distribution of electric field E_z in the x-o-y plane. (c) Simulated transmission coefficients, S_{21}, from TE_{10}^{w} to TE_{10}^{2w} modes, and TE_{10}^{w} to TE_{20}^{2w} modes, when L_1/L varies from 0 to 0.5.

constant of the TE_{n0} mode can be expressed as $\beta^2 = k_0^2 - (n\pi/w_g)^2$, in which k_0 and w_g are the free-space wave number and waveguide width, respectively. Therefore, when $w_g = nw$, we have the same propagation constant β for modes TE_{n0}^{nw} and TE_{10}^{w} within the waveguides of different widths. Figure 2(c) depicts the electric field distribution in the transverse cross section (x-o-z plane) for TE_{10}^{w}, TE_{20}^{w}, and TE_{30}^{w} modes.

Due to matching of the propagation constants for the two modes, we can construct a transition between two waveguides with various cross sections by directly connecting them together, without considering severe reflections at the waveguide junction. For instance, as illustrated in Fig. 3(a), the TE_{10}^{w} and TE_{20}^{2w} modes are generated in the left and right waveguides, respectively, with a width ratio of 1:2, where the glide symmetric ridges are incorporated for the manipulation of mode-dispersion characteristics. Here, the ideal waveguide ports are adopted to excite the desired waveguide modes. Because of the impedance and propagation constant differences between the empty waveguide and periodically loaded waveguide, tapered transitions are employed in our design [see the dotted rectangles in Fig. 3(a)], which can help increase the conversion rate between various waveguide modes and remove unwanted wave reflections. The heights of the ridges are gradually increased from $h_r/3$ to h_r near port 1 and port 2. The simulated electric field distributions are reported in Fig. 3(b), and the perfect conversion can be observed from TE_{10}^{w} to TE_{20}^{2w} modes when passing through the transition.

The mode purity, as an important factor to evaluate the degree of single-mode operation within the waveguide, is analyzed by the simulated transmission coefficients from TE_{10}^{w} to TE_{10}^{2w} and TE_{20}^{2w} modes. Under excitation of the TE_{10}^{w} mode on the left side in Fig. 3(a), the magnitude ratio of output TE_{20}^{2w} and TE_{10}^{2w} modes can be over 25 dB from 10.2 to 12 GHz [see Fig. 3(c)] when L_1/L equals zero, implying that the incident mode is significantly suppressed in this case, and only the TE_{20}^{2w} mode is supported as the carrier wave for single-mode operation. Notably the suffix of S_{21} in Fig. 3(c) represents the conversion rate from the latter to the former mode. For example, $S_{21}[TE_{20}^{2w} - TE_{10}^{w}]$ stands for the magnitude ratio between the output TE_{20}^{2w} mode to the input TE_{10}^{w} mode. This phenomenon is consistent with the theoretical discussions in Fig. 2(d), since the TE_{10}^{w} mode is totally forbidden in this frequency range with $L_1/L = 0$. As L_1/L gradually increases, it gives rise to

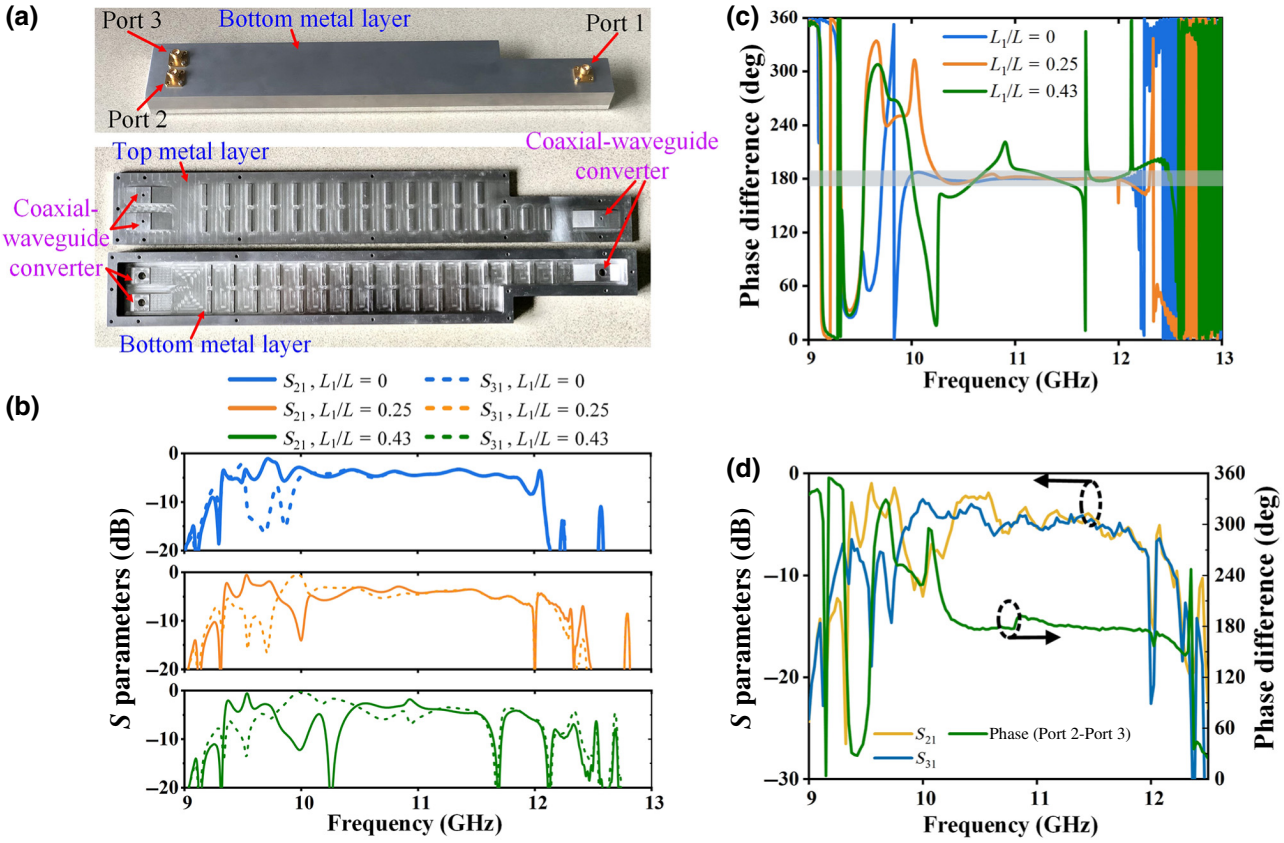

FIG. 4. (a) Photograph of the fabricated TE_{20} mode generator, which is excited by a coaxial probe. (b) Simulated transmission coefficients S_{21} and S_{31} when L_1/L is 0, 0.25, and 0.43. (c) Simulated phase differences between ports 2 and 3 when L_1/L is 0, 0.25, and 0.43. (d) Measured transmission coefficients and phase difference when L_1/L is 0.25.

the reduction of the bandwidth for single high-order mode operation, thanks to the decrease of the band gap in Fig. 2(b). When the ridges are arranged with glide symmetry $L_1/L = 1/2$, the amplitudes of the TE_{10}^{2w} and TE_{20}^{2w} modes are nearly the same. This suggests that the single high-order operation is no longer permitted in this case.

III. RESULTS AND DISCUSSION

To experimentally characterize the phenomenon of single high-order mode operation, we design and fabricate a prototype of the waveguide that only supports the TE_{20}^{2w} mode, as shown in Fig. 4(a). There are two rows and 13 columns of ridges inside the sample. As the launcher of the TE_{20}^{2w} mode, a narrow waveguide that operates only with the TE_{10}^{w} mode is connected on the right for mode conversion, as mentioned in Fig. 3. The dimensions of the waveguide and these periodic ridges are identical to that of the design in Fig. 3(a). The only difference is that the ideal waveguide ports, which are used to stimulate the desired waveguide modes, are replaced by coaxial probes for practical excitation. Because the TE_{20}^{2w} mode can be considered as the combination of two TE_{10}^{w} modes with reversed phase in the transverse cross sections, as shown in Figs. 2(b) and 2(d), the ideal waveguide, port 2 in Fig. 3(a), can be replaced by two independent coaxial probes. Under the conditions of the TE_{20} mode, the signals of these two ports [ports 2 and 3 in Fig. 4(a)] must be out of phase and of uniform amplitude.

The *S* parameters of the three-port network are measured by the network analyzer Agilent N5230C. If port 3 is connected by a matched load, we can measure the transmission coefficient S_{21} from port 1 to port 2. Similarly, we can obtain S_{31} in the same way. Figures 4(b) and 4(c) show the simulated transmission coefficients ($|S_{21}|$ and $|S_{31}|$) and the phase difference ($\angle S_{21} - \angle S_{31}$) for different values of L_1/L. For an ideal TE_{20} mode, S_{21} and S_{31} should be out of phase. The gray region in Fig. 4(c) highlights the range, with $180° \pm 5°$. It is found that the bandwidth with opposite phase starts from 9.9 to 12.1 GHz, when

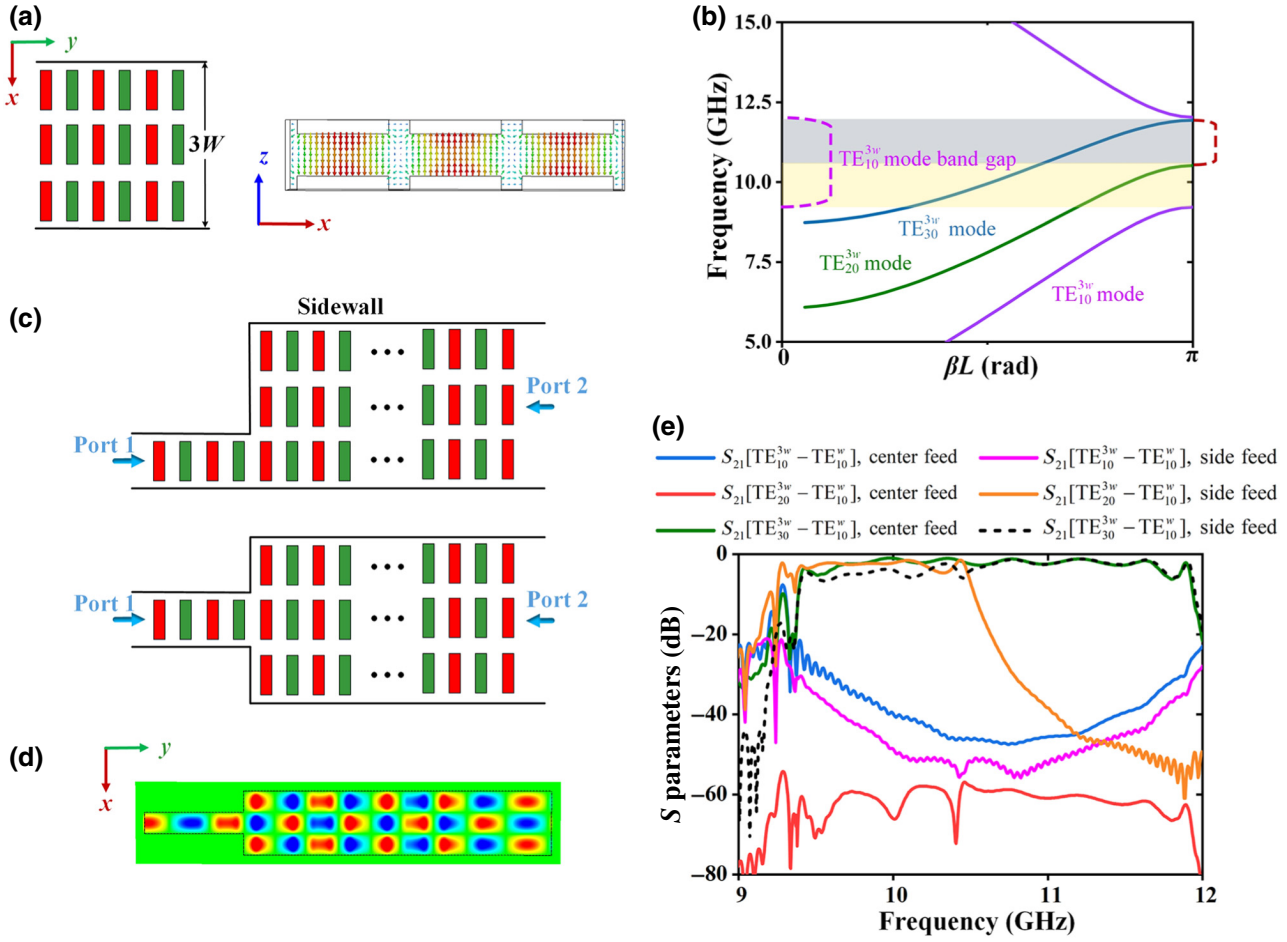

FIG. 5. (a) TE_{30} waveguide and corresponding electric field distribution in the *x-o-z* plane. (b) Dispersion curves of TE_{10}^{3w}, TE_{20}^{3w}, and TE_{30}^{3w} modes with $L_1/L = 0$. (c) TE_{30}^{3w} mode generation with side and central feeding. (d) Distribution of simulated electric field E_z in the *x-o-y* plane with central feeding. (e) Simulated transmission coefficients S_{21} from TE_{10}^{w} to TE_{10}^{3w} modes, TE_{10}^{w} to TE_{20}^{3w} modes, and TE_{10}^{w} to TE_{30}^{3w} modes with $L_1/L = 0$.

$L_1/L = 0$, and then narrows gradually as L_1/L increases. The results are consistent with the theoretical prediction in Fig. 3, since the band gap of the TE_{10} mode reduces with an increase of L_1/L. The measured transmission amplitudes and phases with $L_1/L = 0$ are presented in Fig. 4(d). Obviously, the numerical and experimental results [depicted in Figs. 4(b) and 4(c)] agree closely over the whole frequency range. The subtle discrepancy in performance between Figs. 3 and 4 in various parts can be attributed to the impedance mismatch, since the coaxial feeding structures employed in Fig. 4 have a nearly constant impedance of 50 Ω over the whole operation bandwidth.

The aforementioned method can be easily extended to generate a high-order TE_{n0} mode ($n > 2$) for single-mode operation, which offers a large degree of freedom for mode manipulation within the waveguide. To prove its feasibility, we simply broaden the waveguide width, allowing three ridges to align in the lateral direction, as depicted in Fig. 5(a), and therefore, the TE_{30}^{3w} mode can be supported in this case. As stated before, the TE_{30}^{3w} mode actually has identical dispersion properties to those of TE_{10}^{w} and TE_{20}^{2w} modes in Fig. 5(a). Here, we plot the dispersion curves of the first three modes (TE_{10}^{3w}, TE_{20}^{3w}, and TE_{30}^{3w} modes) with $L_1/L = 0$ in Fig. 5(b). It is clear that, in the band gap of the TE_{10}^{3w} mode, there are two modes, namely, TE_{20}^{3w} and TE_{30}^{3w} modes, that can propagate freely. Moreover, in the gray region of Fig. 5(b), only the TE_{30}^{3w} mode can be supported over that frequency range, as predicted in the previous theoretical analysis.

To further suppress the TE_{20}^{3w} mode and expand the single-mode operation bandwidth, the feeding position should be carefully taken into account. Due to the odd symmetry of the TE_{20} mode at the transverse cross section [see Fig. 2(d)], the modal electric field is supposed to be zero at the center. Therefore, if the waveguide is fed by coaxial probes at this point, the TE_{20} mode can hardly be excited due to the field mismatch. This can be verified by considering central feeding and side feeding in Fig. 5(c). From the simulated mode-conversion rates depicted in Fig. 5(e), it can be found that the TE_{20}^{3w} mode is significantly suppressed with central feeding, and the single-mode operation bandwidth for the TE_{30}^{3w} mode is nearly doubled relative to that of the side-feeding case. Figure 5(d) shows

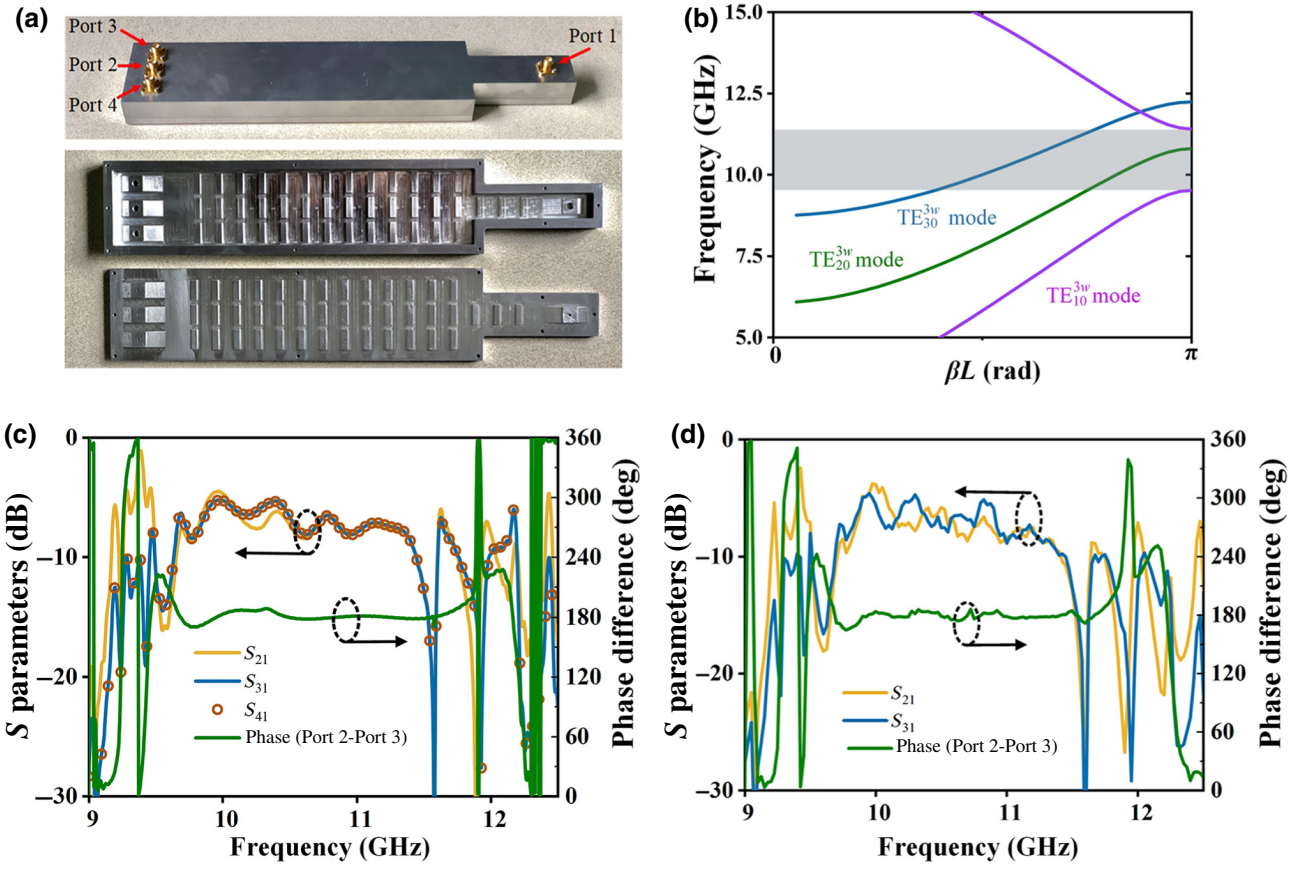

FIG. 6. (a) Photographs of the fabricated TE_{30} mode generator with $L_1/L = 0.25$. (b) Dispersion curves of TE_{10}^{3w}, TE_{20}^{3w}, and TE_{30}^{3w} modes with $L_1/L = 0.25$. (c) Simulated amplitudes of S parameters and phase differences (port 2 and port 3). (d) Measured S_{21} and S_{31}, and the corresponding phase difference between ports 2 and 3.

the electric field distribution of the z component in the x-o-y plane.

Figure 6(a) shows the fabricated sample to verify the capability of band-gap adjustment with reduced glide symmetry. Consistent with the fabricated example in Fig. 4, here L_1/L is selected to be 0.25. Figure 6(b) gives the simulated dispersion diagrams of the designed TE_{30}^{3w} mode waveguide. The simulated transmission amplitudes and phase differences ($\angle S_{21} - \angle S_{31}$, $\angle S_{21} - \angle S_{41}$) are given in Fig. 6(c). It can be seen that the curves of amplitudes (S_{31} and S_{41}) and phase differences ($\angle S_{21} - \angle S_{31}$ and $\angle S_{21} - \angle S_{41}$) overlap, which is attributed to suppression of the TE_{30}^{2w} mode, as shown in Fig. 5(e). The measured results are given in Fig. 6(d). The antiphase range ($180° \pm 5°$) covers the range from 9.9 to 11.7 GHz, which is consistent with the gray region in Fig. 6(b).

IV. CONCLUSIONS

We propose high-order guiding-mode generations with the protection of reduced symmetry. A TE_{20} mode generator is designed in the X band, by loading periodic metallic ridges with reduced glide symmetry in the waveguide. The physical dimensions of the unit cell are optimized to enable an overlap of the low-order-mode band gap and a high-order-mode spectrum, which corresponds to the working band of the TE_{20} mode. Different from the traditional high-order mode generator, the proposed method is capable of modifying the working range independently by reducing the symmetry of the guiding structure. To demonstrate the ability of high-order mode generation, with $n > 2$, one TE_{30} mode generator is achieved by the synergy of the low-order-mode band gaps and feeding network with the symmetry of the TE_{30} mode in the transverse section, which guarantees the unicity of the TE_{30} mode in the working band. The simulated and measured results indicate the unicity of the TE_{n0} mode and the tunability of the bandwidth, which is applicable in various areas where mode elimination or generation are required.

ACKNOWLEDGMENTS

This work is supported, in part, by the National Key Research and Development Program of China (Grants No. 2018YFA0701904, No. 2017YFA0700201, No. 2017YFA0700202, and No. 2017YFA0700203), the National Science Foundation of China (Grants No. 61731010 and No. 61722106), and the 111 Project (Grant No. 111-2-05).

[1] D. M. Pozar, *Microwave Engineering* (John Wiley & Sons, New York, 2009).

[2] S. Deng, D. Pommerenke, T. Hubing, and D. Shin, An experimental investigation of high order mode suppression in TEM cells, IEEE Trans. Electromagn. Compat. **50**, 416 (2008).

[3] I. Arregui, F. Teberio, I. Arnedo, A. Lujambio, M. Chudzik, D. Benito, T. Lopetegi, R. Jost, F. Görtz, J. Gil, et al., High-power low-pass harmonic filters with higher-order TE_{n0} and non-TE_{n0} mode suppression: Design method and multipactor characterization, IEEE Trans. Microw. Theory Tech. **61**, 4376 (2013).

[4] Z. Zhang, J. Luo, and Z. Zhang, Analysis and suppression of high-order mode oscillation in an S-band klystron, IEEE Trans. Plasma Sci. **43**, 515 (2015).

[5] F. Teberio, I. Arregui, A. Gomez-Torrent, E. Menargues, I. Arnedo, M. Chudzik, M. Zedler, F. Görtz, R. Jost, T. Lopetegi, and M. A. G. Laso, High-power waveguide low-pass filter with all-higher-order mode suppression over a wide-band for Ka-band satellite applications, IEEE Microw. Wirel. Co. **25**, 511 (2015).

[6] D. Jia, Q. Feng, Q. Xiang, and K. Wu, Multilayer substrate integrated waveguide (SIW) filters with higher-order mode suppression, IEEE Microw. Wirel. Co. **26**, 1 (2016).

[7] S. G. Tantawi, C. D. Nantista, V. A. Dolgashev, C. Pearson, J. Nelson, K. Jobe, J. Chan, K. Fant, and J. Frisch, High-power multimode X-band rf pulse compression system for future linear colliders, Phys. Rev. Spec. Top. -Accel. Beams. **8**, 527 (2005).

[8] C. D. Nantista and S. G. Tantawi, Multi-moded passive rf pulse compression development at SLAC, AIP Conf. Proc. **569**, 702 (2001).

[9] S. G. Tantawi, C. D. Nantista, G. B. Bowden, K. S. Fant, N. M. Kroll, and A. E. Vlieks, Evaluation of the TE_{12} mode in circular waveguide for low-loss, high-power rf transmission, Phys. Rev. ST Accel. Beams **5**, 082001 (2002).

[10] V. L. Granatstein and W. Lawson, Gyro-amplifiers as candidate RF drivers for TeV linear colliders, IEEE Trans. Plasma Sci. **24**, 648 (1996).

[11] I. Spassovsky, E. S. Gouveia, S. G. Tantawi, B. P. Hogan, W. Lawson, and V. L. Granatstein, Design and cold testing of a compact TE_{10}–TE_{20} mode converter, IEEE Trans. Plasma Sci. **30**, 787 (2002).

[12] G. R. P. Marie, Mode transforming mode transition, U.S. Patent 2859412 (1958).

[13] W. A. Huting and K. J. Webb, Comparison of mode-matching and differential equation techniques in the analysis of a waveguide transitions, IEEE Trans. Microw. Theory Tech. **39**, 280 (1991).

[14] M. Yeddulla, S. Tantawi, J. Guo, and V. Dolgashev, An analytical design and analysis method for a high-power circular to rectangular waveguide mode converter and its applications, IEEE Trans. Microw. Theory Tech. **57**, 1516 (2009).

[15] M. Belaid, R. Martinez, and K. Wu, A mode transformer using fin-line array for spatial power-combiner applications, IEEE Trans. Microw. Theory Tech. **52**, 1191 (2004).

[16] J. Xu, N. C. Zhi, X. Qing, and H. Wei, in *Asia-Pac. Microwave Conf. Proc.* (2011).

[17] W. Peng, J. Liu, and X. Quan, Wideband excitation technology of mode substrate integrated waveguide (SIW) and its applications, IEEE Trans. Microw. Theory Tech. **63**, 1863 (2015).

[18] J. Xu, Z. N. Chen, X. Qing, and W. Hong, 140-GHz-mode dielectric-loaded SIW slot antenna array in LTCC, IEEE Trans. Antennas Propag. **61**, 1784 (2013).
[19] J. Bae, M. Fujita, and K. Mizuno, A W-band overmoded-waveguide oscillator with Gunn diodes, IEEE Trans. Microw. Theory Tech. **49**, 2554 (2000).
[20] S. Matsumoto, I. Ohta, K. Fukada, T. Kawai, K. Iio, and T. Kashiwa, in *Asia-Pac. Microwave Conf. Proc.* (2009).
[21] H. Ikeuchi, T. Kawai, M. Kishihara, and I. Ohta, in *Asia-Pac. Microwave Conf. Proc.* (2012).
[22] H. Ikeuchi, S. Matsumoto, T. Kawai, and I. Ohta, in *IEEE MTT-S Int. Microwave Symp.* (2010).
[23] A. A. Kirilenko, L. A. Rud, and V. I. Tkachenko, Nonsymmetrical H-plane corners for TE10–TEq0 mode conversion in rectangular waveguides, IEEE Trans. Microw. Theory Tech. **54**, 2471 (2006).
[24] A. J. Martinez-Ros, M. Bozzi, and M. Pasian, Double-sided SIW leaky-wave antenna with increased directivity in the E-plane, IEEE Trans. Antennas Propag. **66**, 3130 (2018).
[25] P. J. Crepeau and P. R. Mcisaac, Consequences of symmetry in periodic structures, Proc. IEEE. **52**, 33 (1963).
[26] L. Brillouin, *Wave Propogation in Periodic Structures: Electric Filters and Crystal Lattices* (McGraw-Hill, New York, 1946).
[27] D. A. Watkings, *Topics in Electromagnetic Theory* (John Wiley & Sons, New York, 1958).
[28] R. E. Collin, *Foundations for Microwave Engineering* (McGraw-Hill, New York, 1966).
[29] A. Hessel, H. C. Ming, R. C. M. Li, and A. A. Oliner, Propagation in periodically loaded waveguides with higher symmetries, Proc. IEEE. **61**, 183 (1973).
[30] W. Wang, Z. Zheng, X. Fang, H. Zhang, M. Jin, J. Lu, Q. Luo, and S. Gao, A waveguide slot filtering antenna with an embedded metamaterial structure, IEEE Trans. Antennas Propag. **67**, 2953 (2019).
[31] Q. Huang, W. Wang, W. Jin, and K. Chiang, Ultra-broadband mode filter based on phase-shifted long-period grating, IEEE Photonics Technol. Lett. **21**, 1052 (2019).
[32] A. Hessel and A. Oliner, *Electromagnetic Wave Theory* (Elsevier, New York, 1967).
[33] J. R. Pierce, Coupling of modes of propagation, J. Appl. Phys. **25**, 179 (1954).

Correction: A footnote indicating an additional corresponding author was mistakenly added during production and has been removed. The order of the footnotes has also been adjusted.